

# Solitons in Bose-Einstein Condensates with Attractive Self-Interaction on a Möbius Strip

Huan-Bo Luo<sup>1,2</sup>, Guilong Li<sup>1</sup>, Fu-Quan Dou<sup>3</sup>, Bin Liu<sup>1,\*</sup>, Boris A. Malomed<sup>4,5</sup>, Josep Batle<sup>6,7</sup>, and Yongyao Li<sup>1†</sup>

<sup>1</sup>*School of Physics and Optoelectronic Engineering, Foshan University, Foshan 528000, China*

<sup>2</sup>*Department of Physics, South China University of Technology, Guangzhou 510640, China*

<sup>3</sup>*College of Physics and Electronic Engineering, Northwest Normal University, Lanzhou 730070, China*

<sup>4</sup>*Department of Physical Electronics, School of Electrical Engineering, Faculty of Engineering, Tel Aviv University, Tel Aviv 69978, Israel*

<sup>5</sup>*Instituto de Alta Investigación, Universidad de Tarapacá, Casilla 7D, Arica, Chile*

<sup>6</sup>*Departament de Física UIB and Institut d'Aplicacions Computacionals de Codi Comunitari (IAC3), Campus UIB, E-07122 Palma de Mallorca, Balearic Islands, Spain and*

<sup>7</sup>*CRISP – Centre de Recerca Independent de sa Pobla, sa Pobla, E-07420, Mallorca, Spain*

We study the matter-wave solitons in Bose-Einstein condensate (BEC) trapped on a Möbius strip (MS), based on the respective Gross-Pitaevskii (GP) equation with the mean-field theory. In the linear regime, vortex states are characterized by quantum numbers,  $n$  and  $m$ , corresponding to the transverse and circumferential directions, with the phase structure determined by the winding number (WN)  $m$ . Odd and even values of  $n$  must associate, respectively, with integer and half-integer values of  $m$ , the latter ones requiring two cycles of motion around MS for returning to the initial phase. Using variational and numerical methods, we solve the GP equation with the attractive nonlinearity, producing a family of ground-state (GS) solitons for values of the norm below the critical one, above which the collapse sets in. Vortex solitons with  $n = 1, m = 1$  and  $n = 2, m = 1/2$  are obtained in a numerical form. The vortex solitons with  $n = 1, m = 1$  are almost uniformly distributed in the azimuthal direction, while ones with  $n = 2, m = 1/2$  form localized states. The Vakhitov-Kolokolov criterion and linear-stability analysis for the GS soliton solutions and vortices with  $n = 1, m = 1$  demonstrates that they are completely stable, while the localized states with  $n = 2, m = 1/2$  are completely unstable. Finally, the motion of solitons on the MS and the collision of two solitons are discussed.

## I. INTRODUCTION

Atomic Bose-Einstein condensates (BECs) offer versatile platforms for simulations of various phenomena from condensed-matter physics [1, 2]. Further, BECs are very accurately modelled by Gross-Pitaevskii equations (GPEs), which are derived in the mean-field (MF) approximation and include the inherent collisional nonlinearity [3, 4], providing a comprehensive setting for the studies of one-dimensional (1D) [5–11], two-dimensional (2D) [12–22], and three-dimensional (3D) [23–27] solitons. In particular, 2D systems with the attractive local interactions give rise to degenerate families of *Townes solitons* (TSs, whose norm does not depend on the intrinsic frequency). TSs were originally predicted as spatial solitons in nonlinear optics [28] and recently observed in binary BECs [29, 30]. This experimental result was possible because TSs, although being unstable states, are subject to weak (subexponential) instability against small perturbations, which may be controlled in the experiment (although the growth of the instability eventually leads to the critical collapse, i.e., formation of a singularity after a finite evolution time [31–33]).

In addition to self-trapping on the flat surface, 2D localized states can also appear on curved ones, as recently

demonstrated for solitons [34], vortices [35], and super-solids [36] on spherical surfaces. The electronic states on the pseudosphere [37] have also been reported recently. The subject of the present work is the prediction of 2D solitons – in particular, ones with an intrinsic topological structure – on another well-known curved surface, *viz.*, the Möbius strip (MS) [38, 39]. In this connection, it is relevant to mention that MS-shaped optical patterns (at least, as concerns their polarization structure), that may serve as appropriate traps for atomic BEC, have been predicted and created in a number theoretical and experimental works [40–44]. Photonic Berry-phase states were observed in MS-shaped microcavities [45]. Furthermore, BEC configurations with shapes somewhat similar to MSs were predicted and observed in magnon condensates [46] and atomic BECs [47, 48].

MS, as a non-orientable surface with a single side and edge, has drawn significant attention due to its unique topological properties [49–54], which preclude the application of ordinary periodic boundary conditions (BCs) to physical models based on 2D partial differential equations. Recent theoretical and experimental advances have revealed elementary excitations and novel physical phenomena on MSs in a variety of settings, ranging from molecules [55, 56] and single crystals [57] to optical cavities [41, 58]. These studies bring into the focus effects of the MS's local curvature effects and its unique boundary conditions. In particular, the mean-field model for BEC on MS, based on the respective Gross-Pitaevskii (GP) equations, offers a natural setup for predicting solitons

\*Electronic address: binliu@fosu.edu.cn

†Electronic address: yongyaoli@gmail.com

on curved surfaces, and may also help to improve the understanding of the quantum mechanical behavior in 2D systems with the MS topology.

We use mean-field theory to model the BEC on a MS in order to obtain soliton solutions. Subsequently, in numerical calculations presented in this paper, we handle the specific periodic BCs, introduced by MS, by dint of the finite-element method (FEM). In the linear limit, we numerically solve the Schrödinger equation for MS eigenstates, including ones with embedded vorticity. In the nonlinear regime, we obtain numerical solutions of the GP equation the solitons (including vortical ones) and compare them to results produced by a semi-analytical variational approximation (VA). Finally, we develop the linear stability analysis for the solitons.

The paper is structured as follows. In Sec. II, the model and the linear solution for the eigenstates, including vortices, are introduced. Sec. III presents numerical soliton solutions of the GP equation with the attractive interaction, representing the MS ground state (GS), along with approximate soliton solutions obtained through VA, which are found to closely match the numerical counterparts. Sec. IV reports the numerically found vortex soliton solutions of the GP equation. The stability of the GS and vortex solitons against small perturbations is discussed in Sec. V. In Sec. VI, the motion of solitons on the MS and the collision of two solitons are discussed. Finally, Sec. VII concludes the paper.

## II. THE MODEL AND SOLUTIONS OF THE LINEAR SYSTEM

We consider atomic BEC with attractive interactions, loaded onto MS with width  $2w$  and radius  $r$ , as shown below in Figs. 1-3. By means of scaling, we fix  $r = 2$  and then focus of the value of  $w = 1$ . The Cartesian coordinates on MS are written in a parametric form as

$$\begin{aligned} x(u, v) &= \left(r + wv \cos \frac{u}{2}\right) \cos u, \\ y(u, v) &= \left(r + wv \cos \frac{u}{2}\right) \sin u, \\ z(u, v) &= wv \sin \frac{u}{2}, \end{aligned} \quad (1)$$

where curvilinear coordinates  $u$  and  $v$  take values in intervals  $-\pi \leq u \leq \pi$  and  $-1 \leq v \leq 1$ . This parametrization defines MS centered at the origin of the  $(x, y)$  plane.

In terms of coordinates (1), the MS metric  $g$  and Jacobian determinant  $|J|$  are given by

$$g = \begin{pmatrix} \lambda^2 & 0 \\ 0 & w^2 \end{pmatrix}, \quad |J| = \sqrt{|g|} = w\lambda, \quad (2)$$

where

$$\lambda(u, v) \equiv \sqrt{\left(r + wv \cos \frac{u}{2}\right)^2 + \frac{w^2 v^2}{4}}. \quad (3)$$

Accordingly, the free-space GP equation,  $i\partial\Psi/\partial t = -(1/2)\nabla^2\Psi - |\Psi|^2\Psi$ , constrained onto the MS, takes the form of

$$i\frac{\partial\Psi}{\partial t} = -\frac{1}{2\lambda}\partial_u\left(\frac{1}{\lambda}\partial_u\Psi\right) - \frac{1}{2w^2\lambda}\partial_v(\lambda\partial_v\Psi) - |\Psi|^2\Psi. \quad (4)$$

Applying rescaling to Eqs. (4) and (3), *viz.*,

$$w \equiv (r/2)\tilde{w}, \lambda \equiv (r/2)\tilde{\lambda}, t \equiv (r/2)^2\tilde{t}, \Psi \equiv (2/r)\tilde{\Psi}, \quad (5)$$

these equations are reduced to ones with  $r = 2$ , which is fixed below. Then, we focus on the case of  $w = 1$ , which makes it possible to produce generic results, and drop tildes over the rescaled variables.

Stationary solutions of Eq. (4) with real chemical potential  $\mu$  are sought for in the usual form,

$$\Psi(u, v, t) = \exp(-i\mu t)\psi(u, v), \quad (6)$$

with function  $\psi(u, v)$  satisfying equation

$$\mu\psi = -\frac{1}{2\lambda}\partial_u\left(\frac{1}{\lambda}\partial_u\psi\right) - \frac{1}{2w^2\lambda}\partial_v(\lambda\partial_v\psi) - |\psi|^2\psi. \quad (7)$$

In terms of coordinates (1) and metric coefficient (3), the norm (scaled particle number) and energy (Hamiltonian) of the stationary states are defined as

$$N = \int_{-\pi}^{\pi} du \int_{-1}^1 dv |\psi|^2 w\lambda, \quad (8)$$

$$E = \int_{-\pi}^{\pi} du \int_{-1}^1 dv \left( \frac{w}{2\lambda} |\partial_u\psi|^2 + \frac{\lambda}{2w} |\partial_v\psi|^2 - \frac{w\lambda}{2} |\psi|^4 \right). \quad (9)$$

The stationary wave function  $\psi(u, v)$  needs to satisfy the natural BCs for MS, which are

$$\begin{aligned} \psi(u, v = -1) &= \psi(u, v = 1) = 0, \\ \psi(u = -\pi, v) &= \psi(u = \pi, -v), \end{aligned} \quad (10)$$

that can be easily handled by FEM, see Appendix A for details.

We first address the linearized version of Eq. (7), looking for vortex states as  $\psi_{n,m}(u, v)$ , where  $n = 1, 2, 3, \dots$  is the quantum number in the transverse ( $v$ ) direction, and

$$m = \begin{cases} 0, \pm 1, \pm 2, \pm 3, \dots & \text{if } n \text{ is odd,} \\ \pm \frac{1}{2}, \pm \frac{3}{2}, \pm \frac{5}{2}, \dots & \text{if } n \text{ is even,} \end{cases} \quad (11)$$

is the winding number (WN, alias vorticity, or magnetic quantum number) in the circumferential ( $u$ ) direction. The WN sign indicates if the phase of the wave function increases or decreases as it rotates counterclockwise along the  $u$  direction. Additionally, the vortex state satisfies constraint

$$\psi_{n,m}^*(u, v) = \psi_{n,-m}(u, v), \quad (12)$$

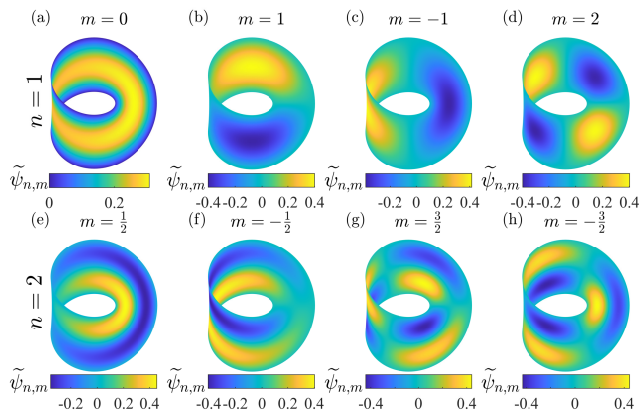


FIG. 1: Real MS eigenstates  $\tilde{\psi}_{n,m}$ , as produced by the linearized equation (7) in the form of the angular standing waves, which are defined as per Eq. (14). The eigenstates are plotted for the lowest values of the transverse and magnetic quantum numbers,  $n$  and  $m$ , which are indicated in panels.

with  $*$  standing for the complex conjugate. The energy spectrum produced by this linear Schrödinger equation was found in a numerical form in Ref. [59], where it was demonstrated that it may be accurately approximated by formula

$$\mu_{n,m} = \frac{\pi^2 n^2}{8w^2} + \frac{m^2}{2r^2}. \quad (13)$$

The spectrum is subject to the exact relation,  $\mu_{n,m} = \mu_{n,-m}$ , which means that the system is always doubly degenerate, except for  $m = 0$ . The degeneracy implies that the linear system admits, instead of the set of vortical eigenmodes  $\psi_{n,\pm m}$ , which are similar to  $\exp(\pm imu)$ , an alternative set in the form of angular standing waves, which are similar to  $\cos(mu)$  and  $\sin(mu)$ , *viz.*,

$$\tilde{\psi}_{n,m} = \begin{cases} (\psi_{n,-m} + \psi_{n,m})/\sqrt{2}, & \text{if } m > 0, \\ \psi_{n,m}, & \text{if } m = 0, \\ i(\psi_{n,m} - \psi_{n,-m})/\sqrt{2}, & \text{if } m < 0. \end{cases} \quad (14)$$

It follows from Eqs. (12) and (14) that wave functions (14) obey the construct  $\tilde{\psi}_{n,m}^* = \tilde{\psi}_{n,m}$ , hence they are real-valued functions. The lowest numerically found eigenstates  $\tilde{\psi}_{n,m}$  are shown in Fig. 1, for  $n = 1$  and  $n = 2$ . As these eigenstates  $\tilde{\psi}_{n,m}$  were studied in detail in Ref. [59], we do not elaborate on them here.

Inverting Eq. (14), one can construct the linear vortex eigenstates  $\psi_{n,m}$  from those  $\tilde{\psi}_{n,m}$ . They are displayed in Fig. 2, in terms of  $|\psi_{n,m}|$  and their phase  $\Theta_{n,m}$ . It is seen that their density distributions are almost identical for the vortex states with the same  $n$ . For odd values of  $n$ , such as  $n = 1$  in Fig. 2,  $m$  is an integer, as in traditional vortex states. This means that, walking once around MS, one will retrieve the initial phase. However, for even values of  $n$ , such as  $n = 2$  in Fig. 2,  $m$  is half-integer, implying that one needs to travel twice around MS for the retrieval of the initial phase.

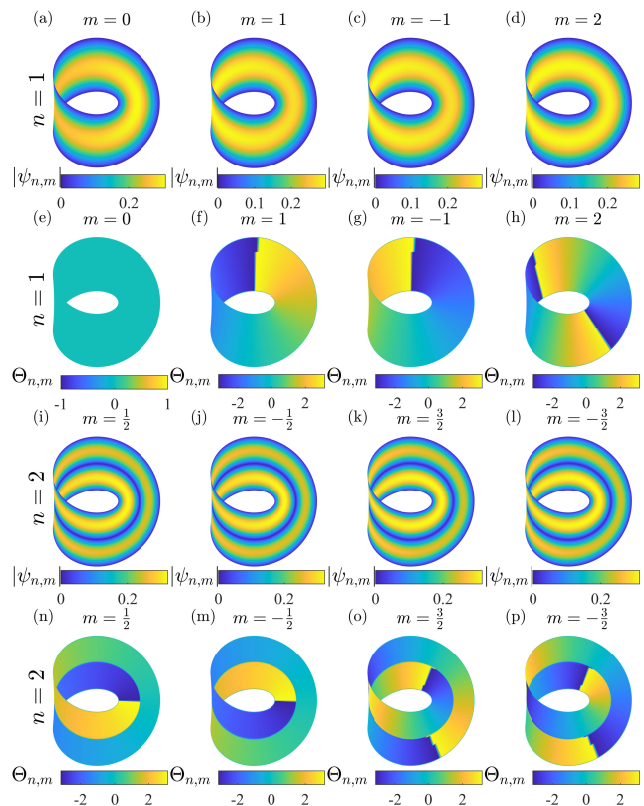


FIG. 2: The density and phase distributions of complex MS vortex states  $\psi_{n,m}$ , as produced by the linearized equation (7). The eigenstates are plotted for values of the transverse and magnetic quantum numbers,  $n$  and  $m$ , which are indicated in panels.

### III. THE NUMERICAL SOLUTION AND VA (VARIATIONAL APPROXIMATION) FOR THE GS SOLITONS OF THE NONLINEAR SYSTEM

Next, we address the complete form of Eq. (7), including the nonlinear term. The use of FEM makes it possible to satisfy BCs (10) in this case too. Here, in the framework of the FEM technique, we use a very efficient Newton's algorithm to obtain the ground-state (GS) solution in the case of the self-attractive nonlinearity in Eq. (7).

To apply the Newton's algorithm, we use the above-mentioned linear eigenstate  $\psi_{1,0}$ , with the corresponding approximate linear eigenvalue  $\mu_{1,0} = 1.23$ , as given by Eq. (13) (recall we set  $w = 1$ ), as the initial guess. Then, the Newton's iterations quickly converge to a numerically accurate solution for the wave function.

By gradually decreasing the chemical potential  $\mu$ , the real GS wave functions for different values of norm  $N$  (8) are obtained and plotted in the Cartesian coordinates  $(x, y, z)$  and MS ones  $(u, v)$  [see Eq. (1)] in Figs. 3(a-d) and (e-h), respectively. In the  $(x, y, z)$  space, the size of the self-trapping area decreases with the increase of  $N$ , due to the strengthening self-attraction. Simultaneously,

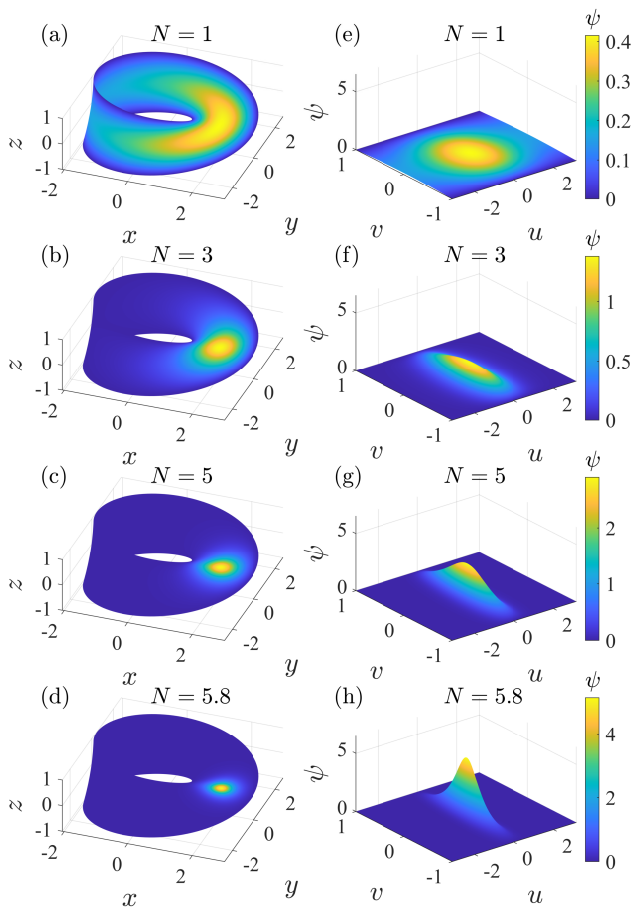


FIG. 3: Real GS solutions of the full nonlinear equation (7), corresponding to quantum numbers ( $n = 1, m = 0$ ), with norms and chemical potential (a, e)  $N = 1$ ,  $\mu = 1.16$ , (b, f)  $N = 3$ ,  $\mu = 0.56$ , (c, g)  $N = 5$ ,  $\mu = -1.31$  and (d, h)  $N = 5.8$ ,  $\mu = -5.40$ .

in the  $(u, v)$  space, the wave-function's peaks become increasingly sharper with the increase of  $N$ .

The self-trapping can be roughly determined by analyzing the interaction-energy term in expression (9):

$$E_{\text{int}} = -\frac{w}{2} \int_{-\pi}^{\pi} du \int_{-1}^1 dv [\lambda(u, v) |\psi|^4]. \quad (15)$$

To minimize  $E_{\text{int}}$ , density  $|\psi|^2$  needs to concentrate at the location where  $\lambda(u, v)$  has its maximum, i.e., around  $u = 0$  and  $v = 1$ , as per Eq. (3). However, due to BC (10), which dictates  $\psi(u, v = 1) = 0$ , the density concentrates around  $u = 0$ , avoiding  $v = 1$ . In the Cartesian coordinates,  $u = 0$  corresponds to  $x = r + uv$ ,  $y = 0$ , and  $z = 0$ , according to Eq. (1). These expectations agree with the numerical findings presented in Fig. 3.

The family of the GS solutions is naturally characterized by the dependence of its norm  $N$  on chemical potential  $\mu$ , which is plotted in Fig. 4(a). Under the action of the self-attraction,  $N$  initially rapidly grows as  $\mu$  decreases (towards  $\mu < 0$ ). Then, the growth saturates,

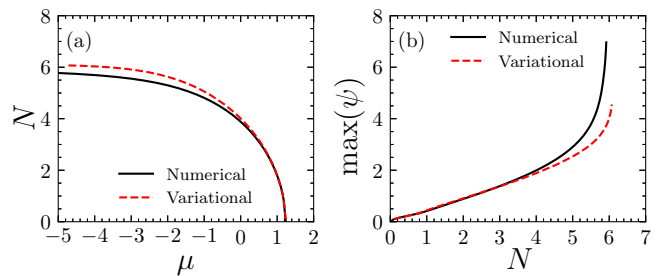


FIG. 4: (a) The norm of the GS solitons obtained from numerical and variational methods vs. the chemical potential  $\mu$ . (b) The amplitude of the GS solitons, obtained in the numerical and variational forms,  $\max(\psi)$ , vs. the norm.

and  $N$  attains the limit value for the extremely narrow soliton,  $N_{\text{TS}}(\mu = -\infty) \approx 5.85$ , which is the commonly known value of the norm of the above-mentioned TSs in the flat 2D space [28, 31, 33]. Indeed, for the solitons with the vanishingly small size the difference between the flat space and MS is negligible. In this connection, it is relevant to mention that the norm of the TSs with embedded integer vorticity  $m$ , found in the 2D flat space [60, 61], increases with the growth of  $m$ , so that  $N_{\text{TS}}^{(m=1)} \approx 24.1$  and  $N_{\text{TS}}^{(m=2)} \approx 44.8$ , in agreement with the approximate analytical prediction [62],

$$\left(N_{\text{TS}}^{(m \geq 1)}\right)_{\text{analyt}} \approx 4\sqrt{3}\pi m. \quad (16)$$

The fact that the plot of  $N(\mu)$  in Fig. 4(a) obeys the *Vakhitov-Kolokolov (VK) criterion*,  $dN/d\mu < 0$ , implies the GS soliton family satisfies the corresponding necessary stability condition [31–33, 63] (the TS family in the flat 2D space is degenerate, with  $dN/d\mu = 0$ , hence they do not obey the VK criterion, and are (weakly) unstable, as mentioned above). The full stability analysis for the GS solitons is reported below in Sec. VII.

A related dependence of the GS-soliton's amplitude,  $\max(\psi)$ , on  $N$  is plotted in Fig. 4(b). The divergence of the amplitude at  $N \rightarrow N_{\text{TS}}$  corroborates the above-mentioned fact that the GS becomes infinitely narrow in this limit.

In addition to the numerical GS solution presented above, it is possible to apply VA with the aim to approximate the solution by a relevant analytical expression. To this end, the variational *ansatz* is chosen in the following tractable form:

$$\psi_{\text{VA}}(u, v) = A(1 - v^2) \text{sech}(au) \exp[-b(v - v_0)^2], \quad (17)$$

with real parameters  $A, a, b > 0$ , and  $v_0$  representing the soliton's amplitude, its inverse widths in the  $u$  and  $v$  directions, respectively, and the offset in the  $v$  direction. Factor  $(1 - v^2)$  is introduced in the *ansatz* to secure that it satisfies the first BC (10). Strictly speaking, the *ansatz* does not satisfy the second BC from Eq. (10); further analysis demonstrates that this BC holds approximately

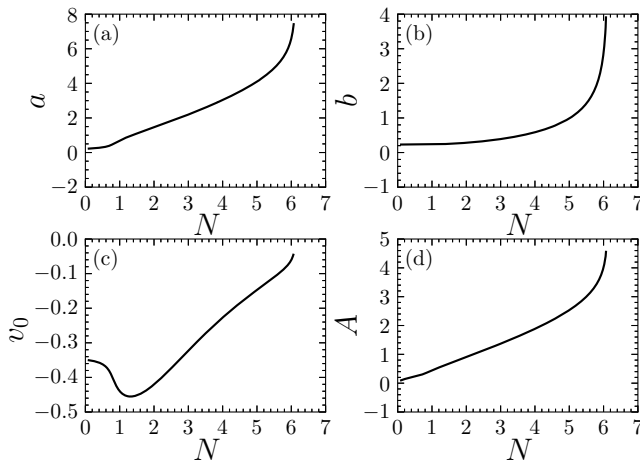


FIG. 5: Parameters of ansatz (17) vs. the norm, as predicted by VA: (a,b) the inverse widths  $a$  and  $b$  in the  $u$ - and  $v$ -directions; (c) offset  $v_0$  in the  $v$ -direction; (d) normalization factor  $A$ .

in the case of  $N > 2$ , in which case the soliton is narrow enough to produce negligibly small values of  $\psi(\pm\pi, v)$ .

Because VA is developed for a given value of  $N$ , amplitude  $A$  is not an independent parameter, being expressed in terms of  $a$ ,  $b$ , and  $v_0$  as per Eq. (8), with  $\psi$  substituted by ansatz (17). The elimination of  $A$  was performed by means of numerical computation of the norm integral (8), as it cannot be performed in an analytical form.

The substitution of the VA ansatz (17) in expression (9) produces the GS-soliton's energy as a function of the variational parameters  $a$ ,  $b$  and  $v_0$ :

$$E_{\text{VA}}(a, b, v_0) = \int_{-\pi}^{+\pi} du \int_{-1}^{+1} dv \left\{ \frac{wa^2 \tanh^2(au)}{2\lambda} \psi_{\text{VA}}^2 + \frac{2}{w} \lambda \left[ \frac{v}{1-v^2} + b(v-v_0) \right]^2 \psi_{\text{VA}}^2 - \frac{w}{2} \lambda \psi_{\text{VA}}^4 \right\}. \quad (18)$$

In the framework of VA, values of the parameters for the GS soliton with fixed norm  $N$  are predicted as those at which energy  $E_{\text{VA}}$ , given by Eq. (18), attains its minimum [recall parameter  $A$  of the VA ansatz (17) is eliminated in favor of  $N$ ]. Under the latter condition, the minimum of expression (18) was found numerically, by means of the simplex method [64, 65].

Dependences of the VA-predicted parameters in ansatz (17) on  $N$  are plotted in Fig. 5, and the respective dependences  $N(\mu)$  and  $\max(\psi)$  vs.  $N$  are shown in Fig. 4. As illustrated in Fig. 4, the curves produced by the VA are very close to their counterparts provided by the numerical results. In particular, they exhibit full overlapping at  $N < 4$ . Naturally, the GS soliton becomes narrower in the  $u$  and  $v$  directions with the increase of  $N$ , while its amplitude increases. The VA solution for the GS soliton does not exist at  $N > 6.06 \equiv (N_{\text{TS}})_{\text{VA}}$ , which is the VA counterpart of the above-mentioned limit value,  $N_{\text{TS}} \approx 5.85$  [the simple VA for the TSs in the flat

2D space yields a coarser VA prediction,  $(N_{\text{TS}})_{\text{VA}} = 2\pi$  [66], while for the TSs with embedded integer vorticity  $m \geq 1$  an analytical approximation is provided by the above-mentioned expression (16)].

We compare the VA-predicted results to their numerically found counterparts in Fig. 6 for norms  $N = 1, 3, 5$ , and 5.8 (the latter value is taken close to the critical one,  $N_{\text{TS}} \approx 5.85$ , above which the GS solitons do not exist, as said above). The corresponding values of the variational parameters are presented in Table I. We conclude that the VA-predicted shape of the GS wave function is very close to its numerical counterparts for  $N < 4$ , while for  $N \geq 4$  the numerically found wave function exhibits stronger localization and a sharper peak. This discrepancy is explained by the fact that the ansatz (17) is not sufficiently accurate for very narrow solitons.

$N$	$a$	$b$	$v_0$	$A$
1	0.701	0.234	-0.440	0.445
3	2.195	0.389	-0.323	1.370
5	4.104	0.987	-0.147	2.533
5.8	5.611	1.962	-0.085	3.445

TABLE I: Values of parameters ( $a, b, v_0, A$ ) in ansatz (17), as produced by VA for values of norm  $N$  presented in Fig. 6.

More detailed comparison of the VA-predicted shapes of the GS solitons and their numerical counterparts is presented in Fig. 7 by means of cross-sections of the solitons along  $v = 0$  and  $u = 0$ . For small values of the norm, such as  $N = 1$ , the discrepancy between the variational and numerical results mainly occurs near  $u = \pm\pi$ , because, as mentioned above, ansatz (17) does not accurately satisfy the second BC in Eq. (10) at  $N < 2$ . At intermediate values of the norm, such as  $N = 3$ , VA agrees well with the numerical solution. Finally,

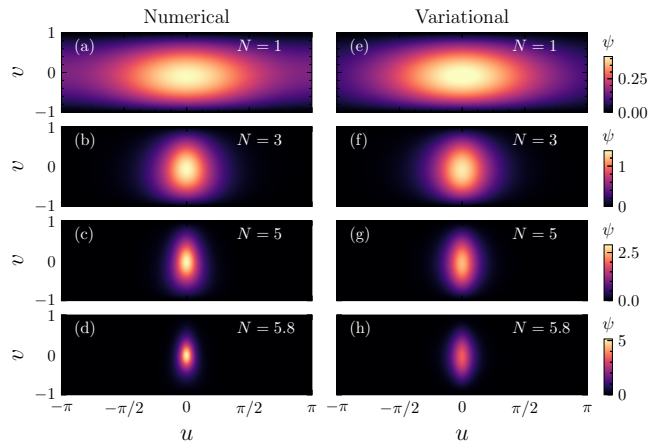


FIG. 6: Comparison of the VA-predicted shapes of the GS solitons at different values of norm  $N$  with the numerically found solitons, for the same values of  $N$ .

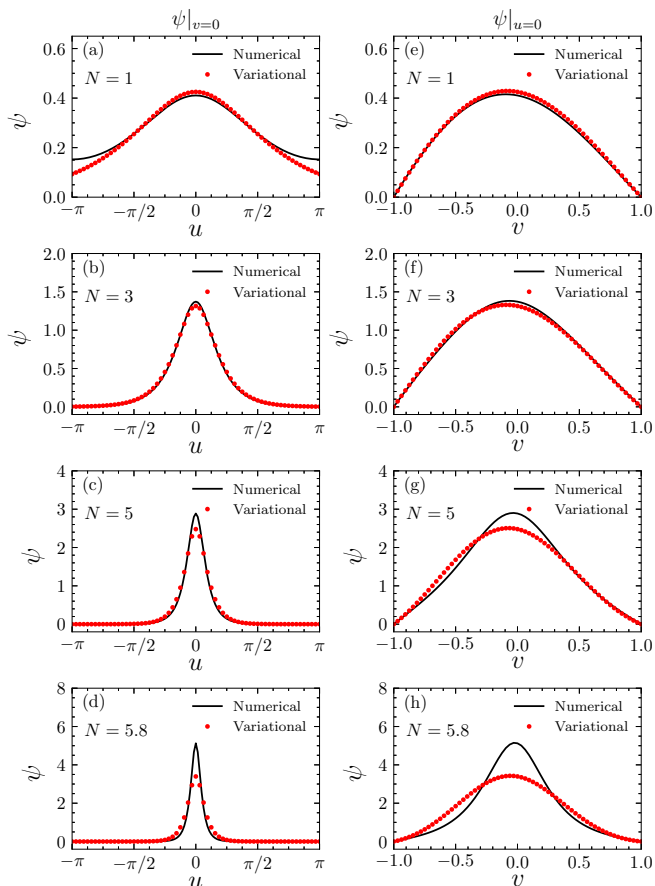


FIG. 7: The comparison of cross sections (along  $v = 0$  and  $u = 0$  in the left and right columns, respectively) of the variational and numerical GS soliton solutions, for different values of norm  $N$ .

as is also mentioned above, at values of  $N$  close to the existence threshold ( $N = N_{\text{TS}}$ ), such as  $N = 5$  and  $N = 5.8$ , the numerical solution exhibits a sharper peak in comparison to the VA prediction, as ansatz (17) is not quite accurate in this case. A general conclusion is that the relatively simple version of VA, based on ansatz (17), produces quite reasonable results.

#### IV. VORTEX SOLITON SOLUTIONS IN THE NONLINEAR SYSTEM

In the previous section, we discussed the properties of GS solitons, including both numerical and variational results. In this section, we discuss the properties of vortex soliton solutions carried by the MS. Here, we focus on the vortex states with  $n = 1, m = 1$  and  $n = 2, m = 1/2$ , as they correspond to the lowest-energy vortex states with integer and half-integer WNs, respectively.

We here again employ the Newton's algorithm within the FEM framework to produce vortex solitons in the nonlinear system. We choose the linear vortex states as

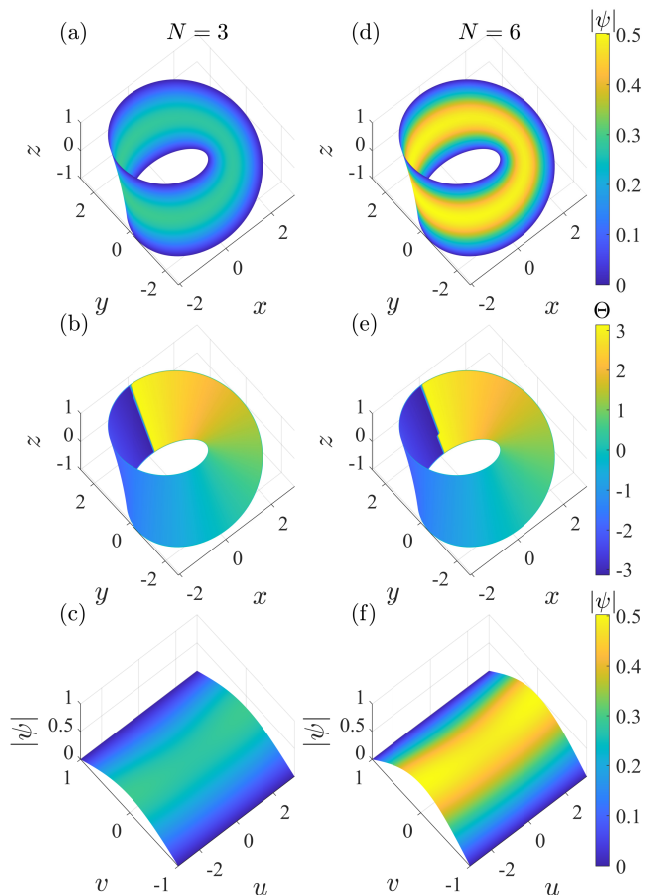


FIG. 8: Vortex soliton solutions of the full nonlinear equation (7), corresponding to quantum numbers  $(n = 1, m = 1)$ , with norms and chemical potential (a-c)  $N = 3$ ,  $\mu = 1.31$ , (d-f)  $N = 6$ ,  $\mu = 1.19$ .

the initial guess for our Newton iteration. The initial guess for  $n = 1, m = 1$  and  $n = 2, m = 1/2$  is  $\psi_{1,1}$  and  $\psi_{2,1/2}$ , respectively. Additionally, the corresponding initial chemical potentials are taken as the linear eigenvalues (13), *viz.*,  $\mu_{1,1} = 1.36$  and  $\mu_{2,1/2} = 4.97$ , respectively.

By gradually decreasing chemical potential  $\mu$ , the numerically found vortex solitons with  $n = 1, m = 1$  and  $n = 2, m = 1/2$  for different norms  $N$  are plotted in Figs. 8 and 9, respectively. As shown in Fig. 8, the vortex solitons with  $n = 1, m = 1$  closely resemble the linear vortex state, with the wave function being nearly uniformly distributed in the  $u$ -direction. Note that, as norm  $N$  increases, the wave functions scale proportionally.

The situation changes for the vortex solitons with  $n = 2, m = 1/2$ . As shown in Figs. 9, the wave function is uniformly distributed, as above, in the  $u$ -direction for  $N = 3$ . However, for  $N = 6$ , the wave function becomes localized, forming four peaks primarily located along the cross-section  $y = 0$ , or, equivalently, at  $u = 0$  and  $u = \pm\pi$ . Thus, there is a phase transition from the uniform state to the localized one.

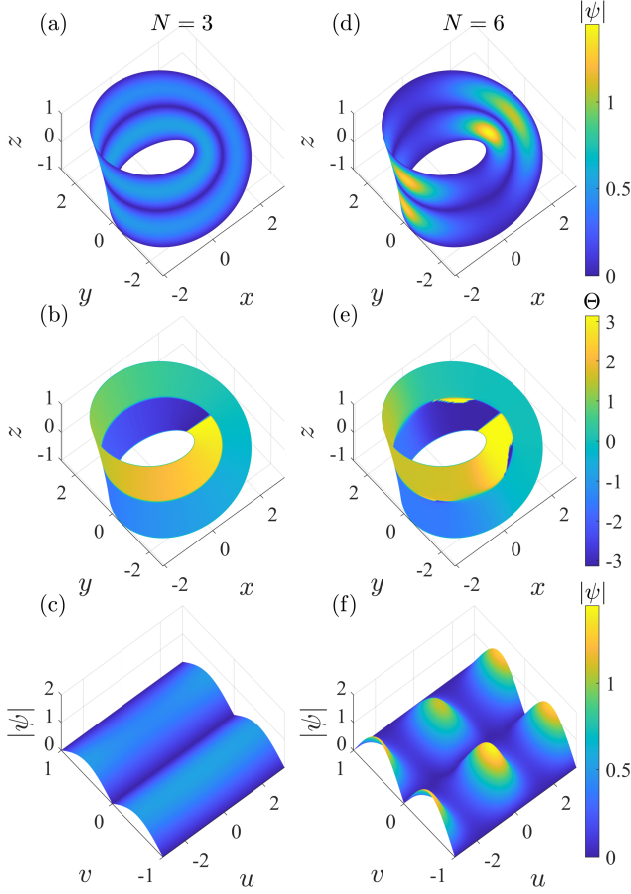


FIG. 9: Vortex soliton solutions of the full nonlinear equation (7), corresponding to quantum numbers  $(n = 2, m = 1/2)$ , with norms and chemical potential (a-c)  $N = 3$ ,  $\mu = 4.79$ , (d-f)  $N = 6$ ,  $\mu = 4.33$ .

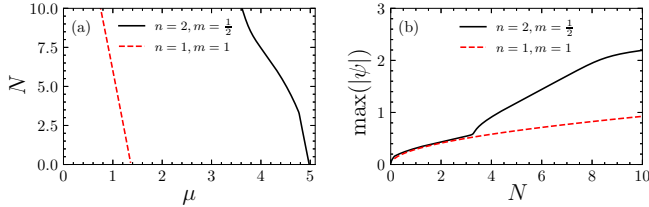


FIG. 10: (a) The norm of the numerically found vortex solitons, with quantum numbers  $n = 1, m = 1$  and  $n = 2, m = 1/2$ , vs. the chemical potential  $\mu$ . (b) The amplitude  $\max(|\psi|)$  of the numerically found vortex solitons, with quantum numbers  $n = 1, m = 1$  and  $n = 2, m = 1/2$ , vs. the norm.

The dependences  $N(\mu)$  and  $\max(|\psi|)$  on  $N$  for vortex solitons with  $n = 1, m = 1$  and  $n = 2, m = 1/2$  are shown in Fig. 10. The fact that the plot of  $N(\mu)$  in Fig. 10(a) obeys the VK criterion,  $dN/d\mu < 0$ , implies that the vortex solitons also satisfy the corresponding necessary stability condition. Nevertheless, the full stability of these modes needs to be confirmed. As  $\mu$

decreases, the norm of the vortex solitons gradually increases. Unlike the GS solitons, the norm of the vortex solitons has no upper limit, and they do not undergo collapse. In Fig. 10(b), the curves of amplitude  $\max(|\psi|)$  for the vortex solitons with  $n = 1, m = 1$  and  $n = 2, m = 1/2$  almost overlap at  $N < 3.3$ . However, at  $N \geq 3.3$ , the two curves diverge, with the one which corresponds to  $n = 2, m = 1/2$  increasing at a faster rate. This fact indicates that  $N = 3.3$  is the critical point at which the vortex soliton with  $n = 2, m = 1/2$  transitions from the uniform state to the localized one.

## V. THE STABILITY ANALYSIS FOR THE SOLITONS

To develop the linear-stability analysis for the real GS solitons, the perturbed ones are taken as

$$\Psi(u, v, t) = e^{-i\mu t} \left[ \psi(u, v) + \alpha(u, v)e^{kt} + \beta^*(u, v)e^{k^*t} \right], \quad (19)$$

where  $\alpha$  and  $\beta$  are small perturbations, and  $k$  is the respective (complex) eigenvalue [the stability implying that all eigenvalues have  $\text{Re}(k) = 0$ ]. Inserting the perturbed solution in Eq. (4) and linearizing, one arrives at the linear eigenvalue problem:

$$\begin{pmatrix} \hat{L} & i\psi^2 \\ -i\psi^{*2} & \hat{L}^* \end{pmatrix} \begin{pmatrix} \alpha \\ \beta \end{pmatrix} = k \begin{pmatrix} \alpha \\ \beta \end{pmatrix}, \quad (20)$$

$$\hat{L} \equiv i\mu + \frac{i}{2\lambda} \partial_u \left( \frac{1}{\lambda} \partial_u \right) + \frac{i}{2w^2\lambda} \partial_v (\lambda \partial_v) + 2i|\psi|^2. \quad (21)$$

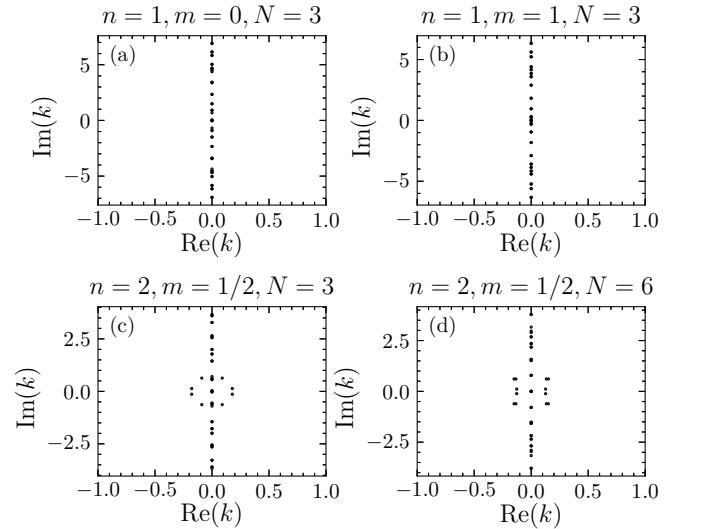


FIG. 11: The linear-stability spectra of the GS solitons with (a)  $n = 1, m = 0, N = 3$ , (b)  $n = 1, m = 1, N = 3$ , (c)  $n = 2, m = 1/2, N = 3$  and (d)  $n = 2, m = 1/2, N = 6$ .

As  $\alpha(u, v)$  and  $\beta(u, v)$  also need to satisfy MS BC (10), the eigenvalue problem (19) was solved by dint of the FEM technique.

Figure 11 presents spectra of the stability eigenvalues for (a) the GS soliton with  $n = 1, m = 0, N = 3$ , (b) the vortex soliton with  $n = 1, m = 1, N = 3$ , (c) the nearly uniform vortex mode with  $n = 2, m = 1/2, N = 3$  and (d) the well-localized vortex mode with  $n = 2, m = 1/2, N = 6$ . The respective stationary states are displayed above in Figs. 3, 8, and 9. The conclusion is that the entire family of the GS solitons is stable, as well as the family of the vortex solitons with quantum numbers  $n = 1, m = 1$ . On the other hand, the modes with  $n = 2, m = 1/2$  are fully unstable.

## VI. MOVING SOLITONS AND THEIR COLLISIONS

The defining characteristics of solitons include their remarkable ability to maintain their shape in the state of motion and collide (quasi-)elastically. Here, we address the motion and collisions of the solitons in the present model.

We consider a soliton moving along the circumferential ( $u$ ) direction of the MS with velocity  $c$ . To this end, we introduce the Galilean transform for the coordinates and derivatives:

$$\xi \equiv u - ct, \quad \tau \equiv t, \quad (22)$$

$$\partial_t = \partial_\tau - c\partial_\xi, \quad \partial_u = \partial_\xi. \quad (23)$$

casting Eq. (4) into the equation for the moving soliton:

$$i\partial_\tau\Psi = ic\partial_\xi\Psi - \frac{1}{2\lambda}\partial_\xi\left(\frac{1}{\lambda}\partial_\xi\Psi\right) - \frac{1}{2w^2\lambda}\partial_v(\lambda\partial_v\Psi) - |\Psi|^2\Psi. \quad (24)$$

Using Eq. (24) and fixing the total particle number  $N$  fixed, we obtain the respective ground-state soliton  $\Psi(\xi, v, \tau)$  by means of the imaginary-time evolution method. Then, we use it as the input in the original reference frame, i.e., in Eq. (4), which produces the ground-state soliton moving with velocity  $c$  along the  $u$ -direction, as shown in Fig. 12(a-d). Here, we set  $N = 3$  and  $c = \pi/8$ , with the respective soliton moving counterclockwise along the MS, with the period of  $T = 2\pi/c = 16$ . At  $t = 0$ , the soliton's center is located at  $x = 2, y = 0, z = 0$ , as shown in Fig. 12(a). After a quarter-period ( $t = 4$ ), it is positioned at  $x = 0, y = 2, z = 0$ , as shown in Fig. 12(c). In the course of the motion, the shape of the soliton remains unchanged.

Next, we consider collisions of two solitons. Using the method outlined above, we prepared another soliton with velocity  $c = -\pi/4$ , particle number  $N = 3$ , and initial position  $x = 0, y = -2, z = 0$ . It moves in the clockwise direction, reaching the position of  $x = 0, y = 2, z = 0$  at the same time,  $t = 4$ , thus initiating the collide. By

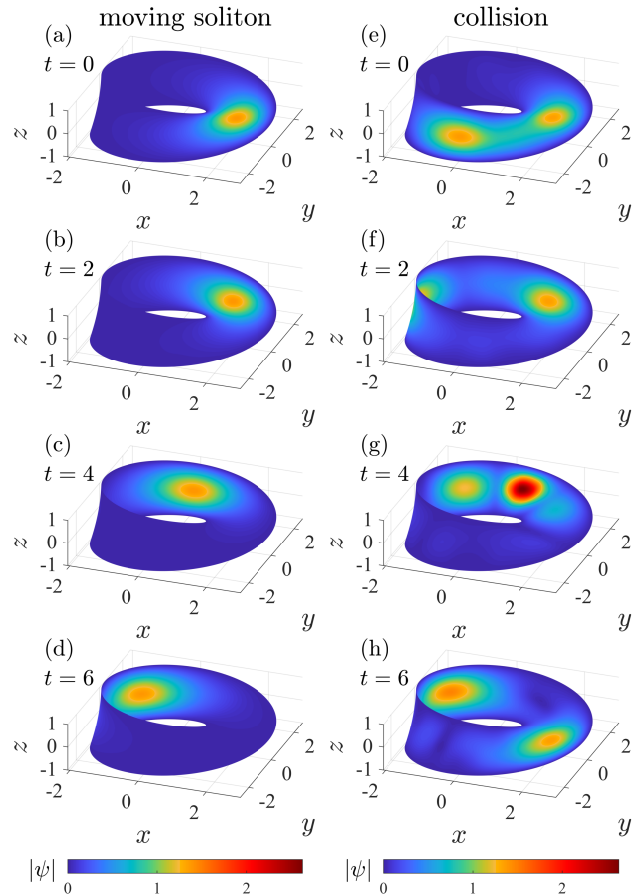


FIG. 12: The evolution of the density distribution for a single moving soliton (a-d) and the collision of two solitons (e-h). In (a), the soliton has velocity  $c = \pi/8$ , particle number  $N = 3$ , being initially located at  $x = 2, y = 0, z = 0$ . In (e), the second soliton is added, with velocity  $c = -\pi/4$ , particle number  $N = 3$ , and initial position  $x = 0, y = -2, z = 0$

superimposing the two solitons and evolving them according to Eq. (4), the collision of the two solitons is displayed in Fig. 12(e-h). As seen in Fig. 12(g), the densities of the two solitons do not directly overlap during the collision. Instead, they form a pattern resembling a standing wave, due to the opposite momenta of the two solitons. Furthermore, as seen in Fig. 12(h), the shapes of the two solitons remain unchanged after the collision, and they continue to move forward at their original velocities. Thus, the collision is quasi-elastic, in spite of the fact that the underlying equation (4) is not integrable.

## VII. CONCLUSION

In this work, we have introduced the 2D GP (Gross-Pitaevskii) equation with the self-attractive nonlinearity on the curved surface in the form of the MS (Möbius strip), as the model for an atomic BEC trapped on such a surface. In the linear limit (the solution for which

was actually reported earlier in Ref. [59]), the vortex states are characterized by quantum numbers,  $n$  and  $m$ , corresponding to the transverse and circumferential directions. The former one,  $n$ , is always integer, while the WN (winding number),  $m$ , is integer for odd  $n$  and *half-integer* for even  $n$  (implying the necessity to perform two round trips along MS to identify the vortical phase). The numerical solution and VA (variational approximation) were used to produce GS (ground-state) soliton solutions of the nonlinear GP equation with self-attraction on the MS. The VA predicts 2D solitons with good accuracy. The attractive cubic nonlinearity leads to the self-compression of the GS solitons and termination of their existence at the critical value of the norm, which coincides with that for the TSs (Townes solitons) in the 2D GP (alias nonlinear Schrödinger) equation in the flat 2D space. However, on the contrary to the unstable TS family in the flat space, the MS geometry lifts the degeneracy of the soliton family and makes them *completely stable* (hence, appropriate for the experimental work), as suggested by the VK (Vakhitov-Kolokolov) criterion and numerical solution of the corresponding linear-stability problem. The vortex solitons with quantum numbers  $n = 1, m = 1$  are stable too, while ones with  $n = 2, m = 1/2$  are unstable.

As an extension of the present work, it is possible to simulate the onset and development of the collapse for the norm exceeding the critical value. Because the collapse leads to catastrophic self-compression of the wave function, it may be expected that it will develop similarly to the known scenario for the nonlinear Schrödinger equation in the flat 2D space [31–33]. It may also be interesting to construct delocalized states, including ones with embedded vorticity, in the framework of the MS GP equation with the repulsive cubic term, while for the attractive one a remaining relevant problem is the modulational instability of delocalized states.

### Acknowledgments

This work was supported by the Guangdong Basic and Applied Basic Research Foundation through grant No. 2023A1515110198, National Natural Science Foundation of China through grants Nos. 12274077, 62405054, 12475014, 12075193, 12475026 and 11905032, Natural Science Foundation of Guangdong Province through grants Nos. 2024A1515030131 and 2021A1515010214, Foundation for Distinguished Young Talents in Higher Education of Guangdong No. 2024KQNCX150, the Research Found of the Guangdong-Hong Kong-Macao Joint Laboratory for Intelligent Micro-Nano Optoelectronic Technology through grant No. 2020B1212030010, and Israel Science Foundation through Grant No. 1695/22.

### Appendix A: Solving the linear eigenstates by dint of the FEM (finite element method)

To apply FEM, we need to define the action  $S = \int_{-1}^{+1} \int_{-\pi}^{+\pi} \mathcal{L} du dv$  corresponding to the linearized equation (7), with the Lagrangian

$$\mathcal{L} = \frac{w}{2\lambda} |\partial_u \psi|^2 + \frac{\lambda}{2w} |\partial_v \psi|^2 - w\lambda\mu |\psi|^2. \quad (\text{A1})$$

As the  $\{u, v\}$  space is a rectangle, we perform its uniform division into the set of  $N_u \times N_v$  small rectangles (*elements*), with intervals in the  $u$  and  $v$ -directions being  $h_u = 2\pi/N_u$  and  $h_v = 2/N_v$ , respectively. Then, the total action is expressed as the sum of actions over the elements, i.e.,

$$S = \sum_{i,j=1}^{N_u, N_v} S_{ij}, \quad S_{ij} = \int_{v_j}^{v_{j+1}} \int_{u_i}^{u_{i+1}} \mathcal{L} du dv, \quad (\text{A2})$$

where the nodes are

$$\begin{cases} u_i = -\pi + h_u(i-1), & i = 1, 2, \dots, N_u + 1, \\ v_j = -1 + h_v(j-1), & j = 1, 2, \dots, N_v + 1. \end{cases} \quad (\text{A3})$$

The wave function at the nodes is defined as  $\psi(u_i, v_i) = \psi_{i,j}$ , with the continuous wave function  $\psi(u, v)$  in intervals  $u_i \leq u \leq u_{i+1}$  and  $v_j \leq v \leq v_{j+1}$  produced by the linear interpolation:

$$\begin{aligned} \psi(u, v) &= \frac{(u_{i+1} - u)(v_{j+1} - v)}{h_u h_v} \psi_{i,j} + \frac{(u - u_i)(v_{j+1} - v)}{h_u h_v} \psi_{i+1,j} \\ &+ \frac{(u_{i+1} - u)(v - v_j)}{h_u h_v} \psi_{i,j+1} + \frac{(u - u_i)(v - v_j)}{h_u h_v} \psi_{i+1,j+1}. \end{aligned} \quad (\text{A4})$$

Higher-order interpolation provides higher accuracy, requiring more nodes in each element. Note that Lagrangian (A1) includes the first derivatives of  $\psi$  with respect to  $u$  and  $v$ . Using the interpolated wave function (A4), we obtain

$$\begin{aligned} \partial_u \psi &= \frac{v_{j+1} - v}{h_u h_v} (\psi_{i+1,j} - \psi_{i,j}) + \frac{v - v_j}{h_u h_v} (\psi_{i+1,j+1} - \psi_{i,j+1}), \\ \partial_v \psi &= \frac{u_{i+1} - u}{h_u h_v} (\psi_{i,j+1} - \psi_{i,j}) + \frac{u - u_i}{h_u h_v} (\psi_{i+1,j+1} - \psi_{i+1,j}). \end{aligned} \quad (\text{A5})$$

Now, substituting the wave function (A4) and its derivatives (A5) in Eqs. (A1) and (A2), and integrating, we obtain:

$$S_{ij} = \begin{pmatrix} \psi_{i,j}^* \\ \psi_{i,j+1}^* \\ \psi_{i+1,j}^* \\ \psi_{i+1,j+1}^* \end{pmatrix}^T (H^{ij} - \mu U^{ij}) \begin{pmatrix} \psi_{i,j} \\ \psi_{i,j+1} \\ \psi_{i+1,j} \\ \psi_{i+1,j+1} \end{pmatrix}, \quad (\text{A6})$$

where the local matrices  $H^{ij}$  and  $U^{ij}$  can be expressed as

$$H^{ij} = \int_{v_j}^{v_{j+1}} \int_{u_i}^{u_{i+1}} \left\{ \frac{w}{2\lambda h_u^2 h_v^2} \begin{pmatrix} v - v_{j+1} \\ v_j - v \\ v_{j+1} - v \\ v - v_j \end{pmatrix} \begin{pmatrix} v - v_{j+1} \\ v_j - v \\ v_{j+1} - v \\ v - v_j \end{pmatrix}^T \right. \\ \left. + \frac{\lambda}{2wh_u^2 h_v^2} \begin{pmatrix} u - u_{i+1} \\ u_{i+1} - u \\ u_i - u \\ u - u_i \end{pmatrix} \begin{pmatrix} u - u_{i+1} \\ u_{i+1} - u \\ u_i - u \\ u - u_i \end{pmatrix}^T \right\} du dv, \quad (\text{A7})$$

and

$$U^{ij} = \int_{v_j}^{v_{j+1}} \int_{u_i}^{u_{i+1}} \frac{w\lambda du, dv}{h_u^2 h_v^2} \\ \times \begin{bmatrix} (u_{i+1} - u)(v_{j+1} - v) \\ (u_{i+1} - u)(v - v_j) \\ (u - u_i)(v_{j+1} - v) \\ (u - u_i)(v - v_j) \end{bmatrix} \begin{bmatrix} (u_{i+1} - u)(v_{j+1} - v) \\ (u_{i+1} - u)(v - v_j) \\ (u - u_i)(v_{j+1} - v) \\ (u - u_i)(v - v_j) \end{bmatrix}^T. \quad (\text{A8})$$

At this point, we need to incorporate the boundary conditions on the Möbius strip (10), which, in terms of the finite-element framework, is:

$$\psi_{i,1} = \psi_{i,N_v+1} = 0, \quad \psi_{N_u+1,j} = \psi_{1,N_v+2-j}. \quad (\text{A9})$$

We need to define  $\{\psi_{i,j}\}$  as a column matrix, with indices ranging over  $i = 1, 2, \dots, N_u$  and  $j = 2, \dots, N_v$  (here, the boundary points are disregarded). In this way, the total action is expressed as

$$S = \{\psi_{i,j}^*\}^T (H - \mu U) \{\psi_{i,j}\}, \quad (\text{A10})$$

where the global matrices  $H$  and  $U$  are assembled by the local matrices  $H^{ij}$  and  $U^{ij}$  [67]. We now invoke the principle of stationary action and vary the action with respect to the nodal values of wavefunction  $\psi_{i,j}^*$ , which leads to the generalized eigenvalue equation,

$$H\{\psi_{i,j}\} = \mu U\{\psi_{i,j}\}. \quad (\text{A11})$$

By numerically solving this equation, we obtain the results for the eigenvalues and eigenstates, which are shown in Fig. 1.

- 
- [1] P. Hauke, F. M. Cucchietti, L. Tagliacozzo, I. Deutsch, and M. Lewenstein, Can one trust quantum simulators?, *Reports on Progress in Physics* **75**, 082401 (2012).
- [2] M. Lewenstein, A. Sanpera, and V. Ahufinger, *Ultracold Atoms in Optical Lattices: Simulating Quantum Many-Body Systems* (Oxford University Press, Oxford, 2012).
- [3] L. P. Pitaevskii and S. Stringari, *Bose-Einstein Condensation* (Oxford University Press, Oxford, 2003).
- [4] Pethick C. J. and H. Smith, *Bose-Einstein Condensation in Dilute Gases* (Cambridge University Press: Cambridge, 2008).
- [5] V. Achilleos, D. Frantzeskakis, P. Kevrekidis, and D. Pelinovsky, Matter-wave bright solitons in spin-orbit coupled Bose-Einstein condensates, *Phys. Rev. Lett.* **110**, 264101 (2013).
- [6] Y. Xu, Y. Zhang, and B. Wu, Bright solitons in spin-orbit-coupled Bose-Einstein condensates, *Phys. Rev. A* **87**, 013614 (2013).
- [7] L. Salasnich and B. A. Malomed, Localized modes in dense repulsive and attractive Bose-Einstein condensates with spin-orbit and Rabi couplings, *Phys. Rev. A* **87**, 063625 (2013).
- [8] V. V. Konotop and L. Pitaevskii, Landau dynamics of a grey soliton in a trapped condensate, *Phys. Rev. Lett.* **93**, 240403 (2004).
- [9] G. Katsimiga, S. I. Mistakidis, G. Koutsokostas, D. Frantzeskakis, R. Carretero-González, and P. Kevrekidis, Solitary waves in a quantum droplet-bearing system, *Phys. Rev. A* **107**, 063308 (2023).
- [10] Y. V. Kartashov, V. V. Konotop, and F. K. Abdullaev, Gap solitons in a spin-orbit-coupled Bose-Einstein condensate, *Phys. Rev. Lett.* **111**, 060402 (2013).
- [11] H.-B. Luo, B. A. Malomed, W.-M. Liu, and L. Li, Tunable energy-level inversion in spin-orbit-coupled Bose-Einstein condensates, *Phys. Rev. A* **106**, 063311 (2022).
- [12] Y. Kartashov, L. Torner, M. Modugno, E. Y. Sherman, B. Malomed, and V. Konotop, Multidimensional hybrid Bose-Einstein condensates stabilized by lower-dimensional spin-orbit coupling, *Phys. Rev. Research* **2**, 013036 (2020).
- [13] C. Qu, L. P. Pitaevskii, and S. Stringari, Magnetic solitons in a binary Bose-Einstein condensate, *Phys. Rev. Lett.* **116**, 160402 (2016).
- [14] H. Sakaguchi, B. Li, and B. A. Malomed, Creation of two-dimensional composite solitons in spin-orbit-coupled self-attractive Bose-Einstein condensates in free space, *Phys. Rev. E* **89**, 032920 (2014).
- [15] V. E. Lobanov, Y. V. Kartashov, and V. V. Konotop, Fundamental, multipole, and half-vortex gap solitons in spin-orbit coupled Bose-Einstein condensates, *Phys. Rev. Lett.* **112**, 180403 (2014).
- [16] L. Salasnich, W. B. Cardoso, and B. A. Malomed, Localized modes in quasi-two-dimensional Bose-Einstein condensates with spin-orbit and Rabi couplings, *Phys. Rev. A* **90**, 033629 (2014).
- [17] X.-Q. Xu and J. H. Han, Spin-orbit coupled Bose-Einstein condensate under rotation, *Phys. Rev. Lett.* **107**, 200401 (2011).
- [18] H.-B. Luo, L. Li, B. A. Malomed, Y. Li, and B. Liu, Energy-level inversion for vortex states in spin-orbit-coupled Bose-Einstein condensates, *Phys. Rev. A* **109**, 013326 (2024).
- [19] H.-B. Luo, B. A. Malomed, W.-M. Liu, and L. Li, Bessel vortices in spin-orbit-coupled binary Bose-Einstein condensates with Zeeman splitting, *Communications in Nonlinear Science and Numerical Simulation* **115**, 106769

- (2022).
- [20] G. Li, X. Jiang, B. Liu, Z. Chen, B. A. Malomed, and Y. Li, Two-dimensional anisotropic vortex quantum droplets in dipolar Bose-Einstein condensates, *Frontiers of Physics* **19**, 22202 (2024).
- [21] Y. Li, Z. Chen, Z. Luo, C. Huang, H. Tan, W. Pang, and B. A. Malomed, Two-dimensional vortex quantum droplets, *Phys. Rev. B* **98**, 063602 (2018).
- [22] X. Jiang, Z. Fan, Z. Chen, W. Pang, Y. Li, and B. A. Malomed, Two-dimensional solitons in dipolar Bose-Einstein condensates with spin-orbit coupling, *Phys. Rev. A* **93**, 023633 (2016).
- [23] Y.-C. Zhang, Z.-W. Zhou, B. A. Malomed, and H. Pu, Stable solitons in three dimensional free space without the ground state: self-trapped Bose-Einstein condensates with spin-orbit coupling, *Phys. Rev. Lett.* **115**, 253902 (2015).
- [24] Y. Zhao, Q. Huang, T. Gong, S. Xu, Z. Li, and B. A. Malomed, Three-dimensional solitons supported by the spin-orbit coupling and Rydberg-Rydberg interactions in  $\mathcal{PT}$ -symmetric potentials, *Chaos, Solitons & Fractals* **187**, 115329 (2024).
- [25] B. Malomed, *Multidimensional Solitons*, AIP Publishing, Melville, NY, 2022.
- [26] G. Li, Z. Zhao, X. Jiang, Z. Chen, B. Liu, B. A. Malomed, and Y. Li, Strongly Anisotropic Vortices in Dipolar Quantum Droplets, *Phys. Rev. Lett.* **133**, 053804 (2024).
- [27] H.-B. Luo, L. Li, and W.-M. Liu, three-Dimensional Skyrmions with Arbitrary topological number in a Ferromagnetic Spin-1 Bose-einstein condensate, *Scientific Reports* **9**, 18804 (2019).
- [28] R. Y. Chiao, E. Garmire, and C. H. Townes, Self-trapping of optical beams, *Phys. Rev. Lett.* **13**, 479 (1964).
- [29] B. Bakkali-Hassani, C. Maury, Y.-Q. Zou, É. Le Cerf, R. Saint-Jalm, P. C. M. Castilho, S. Nascimbene, J. Dalibard, and J. Beugnon, Realization of a Townes soliton in a two-component planar Bose gas, *Phys. Rev. Lett.* **127**, 023603 (2021).
- [30] C.-A. Chen and C.-L. Hung, Observation of scale invariance in two-dimensional matter-wave townes solitons, *Phys. Rev. Lett.* **127**, 023604 (2021).
- [31] L. Bergé, Wave collapse in physics: principles and applications to light and plasma waves, *Phys. Rep.* **303**, 259-370 (1998).
- [32] C. Sulem and P.-L. Sulem, *The Nonlinear Schrödinger Equation: Self-Focusing and Wave Collapse* (Springer, New York, 1999).
- [33] G. Fibich, *The Nonlinear Schrödinger Equation: Singular Solutions and Optical Collapse* (Springer, Heidelberg, 2015).
- [34] A. Tononi, G. Astrakharchik, and D. Petrov, Gas-to-soliton transition of attractive bosons on a spherical surface, *AVS Quantum Science* **6**, 023201 (2024).
- [35] A. Tononi, L. Salasnich, and A. Yakimenko, Quantum vortices in curved geometries, *AVS Quantum Sci.* **6**, 030502 (2024).
- [36] J. Sánchez-Baena, R. Bombín, and J. Boronat, Ring solids and supersolids in spherical shell-shaped dipolar Bose-Einstein condensates, *Phys. Rev. Research* **6**, 033116 (2024).
- [37] J. Furtado, Electronic states in a quantum Beltrami surface, *Physics Letters A* **483**, 129065 (2023).
- [38] Y.-L. Wang, H. Zhao, H. Jiang, H. Liu, and Y.-F. Chen, Geometry-induced monopole magnetic field and quantum spin Hall effects, *Phys. Rev. B* **106**, 235403 (2022).
- [39] N. Zhao, H. Dong, S. Yang, and C. P. Sun, Observable topological effects in molecular devices with Möbius topology, *Phys. Rev. B* **79**, 125440 (2009).
- [40] I. Freund, Cones, spirals, and Möbius strips, in elliptically polarized light, *Opt. Commun.* **249**, 7-22 (2005).
- [41] T. Bauer, P. Banzer, E. Karimi, S. Orlov, A. Rubano, L. Marrucci, E. Santamato, R. W. Boyd, and G. Leuchs, Observation of optical polarization Möbius strips, *Science* **347**, 964-966 (2015).
- [42] E. Pisanty, G. J. Machado, V. Vicuña-Hernández, A. Picón, A. Celi, J. P. Torres and M. Lewenstein, Knotting fractional-order knots with the polarization state of light, *Nature Phot.* **13**, 569-574 (2019).
- [43] K. Y. Bliokh, M. A. Alonso, and M. R. Dennis, Geometric phases in 2D and 3D polarized fields: geometrical, dynamical, and topological aspects, *Rep. Prog. Phys.* **82**, 122401 (2019).
- [44] Q. Wang, C.-H. Tu, Y.-N. Li, and H.-T. Wang, Polarization singularities: Progress, fundamental physics, and prospects, *APL Photonics* **6**, 040901 (2021).
- [45] J. Wang, S. Valligatla, Y. Yin, L. Schwarz, M. Medina-Sánchez, S. Baunack, C. H. Lee, R. Thomale, S. Li, V. M. Fomin, L. Ma, and O. G. Schmidt, Experimental observation of Berry phases in optical Möbius-strip microcavities. *Nature Photonics* **17**, 120-125 (2023).
- [46] S. O. Demokritov, A. A. Serga, V. E. Demidov, B. Hillebrands, M. P. Kostylev, and B. A. Kalinikos, Experimental observation of symmetry-breaking nonlinear modes in an active ring, *Nature* **426**, 159-162 (2003).
- [47] Y. K. Liu, S.-J. Yang, G.-H. Yang, and J.-J. Zhang, Interlocked knot in spinor Bose-Einstein condensates, *Chaos, Solitons & Fractals* **140**, 110209 (2020).
- [48] C.-H. Li, Y.-Q. Yan, S.-W. Feng, S. Choudhury, D. B. Blasing, Q. Zhou, and Y. P. Chen, Bose-Einstein condensate on a synthetic topological hall cylinder, *PRX Quantum* **3**, 010316 (2022).
- [49] N. Nishiguchi and M. N. Wybourne, Phonon modes in a Möbius band, *J. Physics Communications* **2**, 085002 (2018).
- [50] K. Flouris, M. M. Jimenez, and H. J. Herrmann, Curvature-induced quantum spin-hall effect on a Möbius strip, *Phys. Rev. B* **105**, 235122 (2022).
- [51] L. Monteiro, C. Almeida, and J. Silva, Dirac fermions on wires confined to the graphene Möbius strip, *Phys. Rev. B* **108**, 115436 (2023).
- [52] Y. Liu, L.-R. Ding, A.-L. He, and Y.-F. Wang, Quantum transport in Chern insulators on Möbius strips, *Journal of Physics: Condensed Matter* **32**, 505501 (2020).
- [53] L.-T. Huang and D.-H. Lee, Topological insulators on a Möbius strip, *Phys. Rev. B* **84**, 193106 (2011).
- [54] X. Wang, X. Zheng, M. Ni, L. Zou, and Z. Zeng, Theoretical investigation of Möbius strips formed from graphene, *Applied Physics Letters* **97** (2010).
- [55] D. M. Walba, R. M. Richards, and R. C. Haltiwanger, Total synthesis of the first molecular Möbius strip, *Journal of the American Chemical Society* **104**, 3219 (1982).
- [56] G. Ouyang, L. Ji, Y. Jiang, F. Würthner, and M. Liu, Self-assembled Möbius strips with controlled helicity, *Nature Communications* **11**, 5910 (2020).
- [57] S. Tanda, T. Tsuneta, Y. Okajima, K. Inagaki, K. Ya-

- maya, and N. Hatakenaka, A Möbius strip of single crystals, *Nature (London)* **417**, 397 (2002).
- [58] J. Kreismann and M. Hentschel, The optical möbius strip cavity: Tailoring geometric phases and far fields, *Europhysics Letters* **121**, 24001 (2018).
- [59] Z. Li and L. Ram-Mohan, Quantum mechanics on a Möbius ring: Energy levels, symmetry, optical transitions, and level splitting in a magnetic field, *Phys. Rev. B* **85**, 195438 (2012).
- [60] V. I. Kruglov and R. A. Vlasov, Spiral self-trapping propagation of optical beams, *Phys. Lett. A* **111**, 401-404 (1985).
- [61] V. I. Kruglov, Yu. A. Logvin, and V. M. Volkov, he theory of spiral laser beams in nonlinear media, *J. Mod. Phys.* **39**, 2277-2291 (1992).
- [62] J. Qin, G. Dong, and B. A. Malomed, Stable giant vortex annuli in microwave-coupled atomic condensates, *Phys. Rev. A* **94**, 053611 (2016).
- [63] N. G. Vakhitov and A. A. Kolokolov, Stationary solutions of the wave equation in a medium with nonlinearity saturation, *Radiophys. Quantum Electron.* **16**, 783-789 (1973).
- [64] R. E. Stone and C. A. Tovey, The simplex and projective scaling algorithms as iteratively reweighted least squares methods, *SIAM Review* **33**, 220-237 (1991).
- [65] J. C. Lagarias, J. A. Reeds, M. H. Wright, and P. E. Wright, Convergence properties of the Nelder-Mead simplex method in low dimensions, *SIAM J. Optim.* **9**, 1 (1998).
- [66] M. Desaix, D. Anderson, and M. Lisak, Variational approach to collapse of optical pulses, *J. Opt. Soc. Am. B* **8**, 2082-2086 (1991).
- [67] L. R. Ram-Mohan, *Finite Element and Boundary Element Applications in Quantum Mechanics* (Oxford U. P., Oxford, UK, 2002).